Int. J. Electrochem. Sci., 15 **(2020)** 6629 – 6644, doi: 10.20964/2020.07.39

International Journal of
ELECTROCHEMICAL
SCIENCE
www.electrochemsci.org

Research on Theoretically Modelling and Quantitatively Calculating Stray Current Corrosion in a Subway System

Zhichao Cai[*], *Xianwei Zhang, Jing Zhang*

School of Electrical and Automation Engineering, East China Jiaotong University, Nanchang 330013, China;
[*]E-mail: czchebut@foxmail.com

Received: 6 October 2019 / *Accepted:* 30 March 2020 / *Published:* 10 June 2020

To investigate the effect of stray current in subways on the corrosion of buried pipelines near tracks, a 3D-finite element method (FEM) model of stray current distribution for one subway interval was established. Under the operation conditions of subway vehicles, the stray current distribution in the area and its interference with a buried pipeline were analysed and discussed. The calculation found that the area of the buried pipeline corrosion area (anodic area) changed depending on the subway vehicle mode of operation. Corrosion predictions of buried metals with different burial depths were carried out to simulate the corrosion rules of metal anodes under a DC stray current environment. A metal mass loss analysis shows that the mass loss of the metal due to corrosion is inversely proportional to the buried depth of the metal specimen. The established proportional experimental FEM model accurately verified the experimental results. Stray current corrosion modelling and quantitative calculation methods can provide important technical guidance for the health assessment of buried metal corrosion.

Keywords: stray current, FEM, corrosion, quantitative calculation

1. INTRODUCTION

Stray current, especially DC stray current, arising from electrified traction systems, high-voltage power lines or other sources, can induce serious corrosion on metal infrastructures, including reinforced concrete structures, underground cables, and buried pipelines; moreover, corrosion can seriously reduce the service lives of the above infrastructures [1-3]. As shown in Figure 1, in a subway system, the DC traction current provided by traction power substations is transmitted to the subway vehicle via a pantograph-catenary system and provides energy to the subway vehicle. As the running rail cannot be totally isolated from the soil, a part of the traction current leaks into the surrounding soil, which is called stray current [4-6]. Partial stray current flows through buried pipelines (low resistance) placed in the neighbourhoods of railways, and the metals become electrodes in the soil electrolyte environment under the action of stray current. The anodic area of the buried pipeline metal corrodes

away due to the loss of electrons [7-8]. The problem of stray current corrosion is currently a worldwide concern. Subway companies pay high costs for stray current prevention and control every year. In the UK, for example, approximately 600 million euros per annum is spent on the maintenance of transport infrastructure [9]. However, if there are untimely or missed inspections, stray current corrosion will still cause accidents such as buried pipeline leakage. Corrosion and leakage accidents have occurred many times in buried pipelines parallel to DC-powered electric rail transit lines in Shanghai [10]. Therefore, research is necessary to establish an effective method to analyse the stray current corrosion mechanism and evaluate the corrosion status.

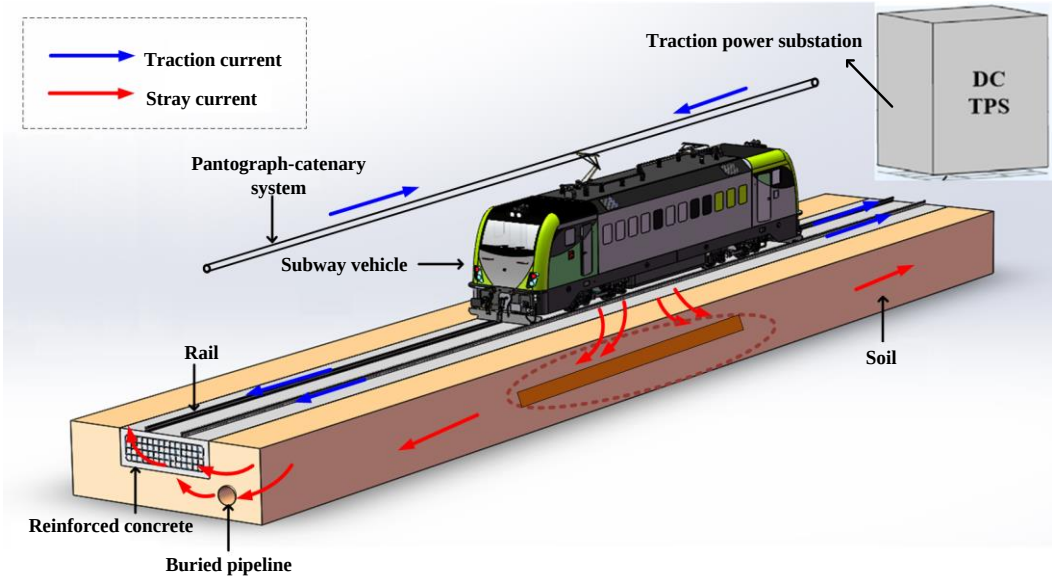

Figure 1. Schematic of stray current leakage in subway system

In recent years, many studies have used stray current distribution models [11-21] to indirectly evaluate the degree of corrosion and damage caused by stray currents. Some mathematical analysis models (a resistance network calculation model [11-14], an electric field model [15], and a hemispherical electrode model [16]) have been established to calculate the size and distribution of stray currents by analysing influencing factors. With the application of simulation software towards the stray current problem, some physical simulation models that have been built through software (CEDGS [17,18], COMSOL [19], Simulink [20,21]) have strong adaptability and computing power. The above models provide effective tools for analysing and calculating the stray current and the stray current distribution, respectively. However, the distribution law of stray current is only an intermediate link to solve the corrosion problem. A more direct analysis method is needed to study the problem of stray current corrosion. The essence of stray current corrosion is the electrochemical reaction of metals [7]. The existing analysis models of stray current distribution cannot directly analyse the corrosion laws of metals. The metal corrosion caused by stray current is usually caused by the coupling of various factors, such as external stress, ionic concentration, pH value of the soil, and electrochemical reactions. Therefore, many studies, especially metal corrosion test studies, mostly analyse the corrosion problems caused by stray currents based on the influence of various physical factors.

An electrochemical experiment method is the main approach for studying metal corrosion under the conditions of multiple physical factors. During the experiment, the actual metal corrosion

environment was simulated by changing the current density [10, 22, 23], temperature [24], external stress [25], ion concentration (Cl^-, HCO_3^-, SO_4^{2-}) [26, 27], pH value [28] and other factors of the simulated soil environment. Then, the corrosion rule of the metal specimen under the action of single or multiple factors was analysed. Compared with the traditional field test method, the electrochemical experiment method is concise and quick. During the experiment, the rate and corrosion rule of metal corrosion are usually studied by polarization curve technology [29, 30], corrosion morphology analysis technology [31], and corrosion product analysis technology [24, 32] and also by a weight loss method [33]. At present, the study of the stray current distribution law and the stray current corrosion mechanism are not fully combined. In addition, the distribution of stray currents and metal corrosion caused by stray currents are random in a subway system. The existing corrosion experiments cannot truly reflect the metal corrosion area in the stray current environment of the subway and quantitatively calculate the metal corrosion mass loss.

In this paper, the proposed 3D-finite element model proposed in this paper solves the above two problems: 1. simulating the stray current distribution under dynamic traction conditions of a subway vehicle and 2. simulating the actual corrosion area of the metal and quantitatively calculating the amount of metal corrosion. The detailed arrangement for the rest of this paper is as follows. The problem of stray current leakage in the subway is proposed, and a 3D-dynamic FEM modelling analysis is performed for the subway interval in Section 2. An N20 carbon steel experiment simulating stray current corrosion and the corresponding 3D-FEM modelling are carried out in Section 3 and Section 4, respectively. The experimental and simulated corrosion rates and corrosion laws are compared and analysed in detail in Section 5. Finally, Section 6 summarizes the content of the paper.

2. DESCRIPTION OF THE PROBLEM AND THEORETICAL MODELLING

The geometry to be studied is a typical subway space interval of Guangzhou Metro, as shown in Figure 2(a). The dimensions of the subway interval under study are set to 1500 × 300 × 200 m (L/W/H). Two stations are located at both ends of the subway interval. There is a subway track at the centre of the ground in the above interval, and a buried pipeline is laid parallel (15 m to the right and 10 m below) to the track. The subway vehicle runs from station 2 to station 1, and its traction current and running velocity are collected from actual data, as shown in Figure 3. The main purpose is to study the interference of the stray current, which is leaked from the track, on the buried pipeline. COMSOL Multiphysics software was selected for modelling, the FEM model was established according to the geometric dimensions, and the meshing of the models is shown in Figure 2(b). The accuracy of the FEM model depends on the degree of mesh generation, but the more detailed the mesh generation, the lower the computational efficiency. Under the premise of satisfying both calculation accuracy and efficiency, the geometric model was finally divided into 734037 tetrahedra, 22000 pyramids, 71282 prisms, 6000 hexahedra, 65858 triangles, 40430 quads, 28727 edge elements and 104 vertex elements.

Due to the nature of the soil conductive medium, only the electrical conductivity of the soil is considered in the research process, and other factors such as the concentration gradient in the soil are ignored [34]. The soil is assumed to have only the normal ohmic resistivity effect. The potential at the

bottom of the soil and at the station (current return point) is set to 0 V. The potential field is formed in the soil range, and the stray current is transmitted in the soil space, which can be described by the Laplace equation [15]:

$$\nabla^2\phi = 0 \quad (1)$$

The electric field strength E in the soil can be obtained from the negative potential gradient:

$$E = -\nabla\phi \quad (2)$$

The current density J in the soil electrolytes meets Ohm's law as follows:

$$J = \sigma E \quad (3)$$

where σ is the electrical conductivity of the soil.

Both the soil and buried pipelines are set to constant conductivities, which are 1.5 S/m and 1E7 S/m, respectively. For simplicity, the electrical conductivity of metals such as the tracks are also set to 1E7 S/m.

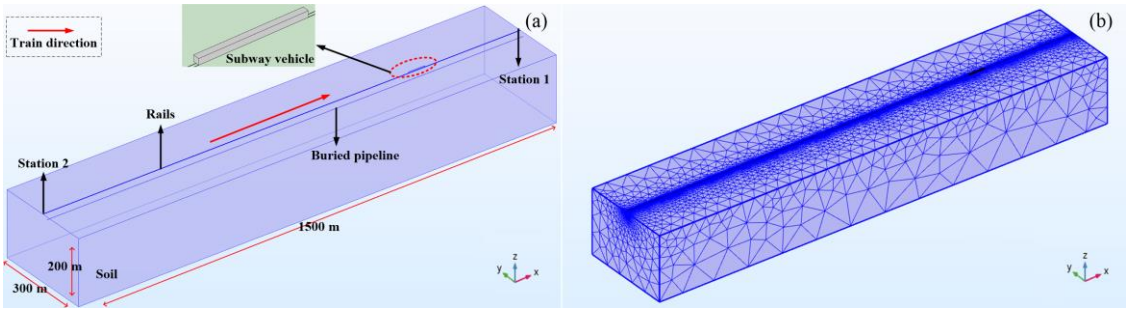

Figure 2. Geometry and meshing of the subway interval

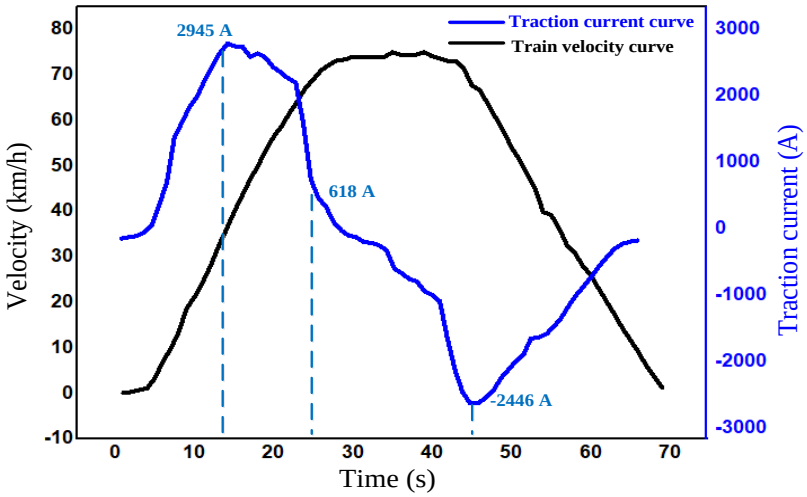

Figure 3. Subway vehicle operating conditions (velocity and traction current)

Figure 4 shows the cloud diagrams of the electric potential distribution in the longitudinal section of the subway interval during the subway vehicle at 13 s, 25 s and 45 s (corresponding to three different operating modes of the subway vehicle: acceleration, constant speed and deceleration). It can be clearly found that the area near the subway vehicle has the highest electric potential, which

gradually decreases as it moves away from the subway vehicle location. Comparing Figure 4(a), Figure 4(b) and Figure 4 (c), it can be found that the traction current of the subway vehicle determines the potential distribution. The traction currents of the subway vehicle at 13 s, 25 s and 45 s are 2945 A, 618 A and 2446 A, respectively (To facilitate comparison, the traction current takes a positive value during the simulation). Correspondingly, the potentials at one metre directly below the subway vehicle position are 0.52 V, 0.08 V, 0.43 V. According to the EN50162-2004 standard [35], if the forward potential exceeds 0.3 V, protective measures should be taken. At the same time, the maximum potential of the buried pipeline to the soil is 0.075 V, 0.012 V, and 0.061 V. Although the potential value of the pipeline to soil is far less than the protection standard, the long-term accumulation effect of stray current cannot be ignored.

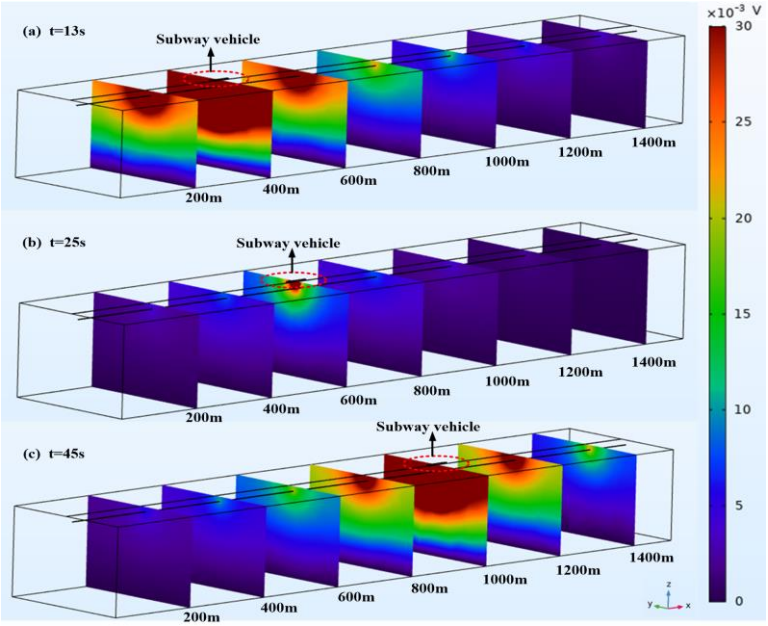

Figure 4. Electric potential distribution in the longitudinal section of the subway interval

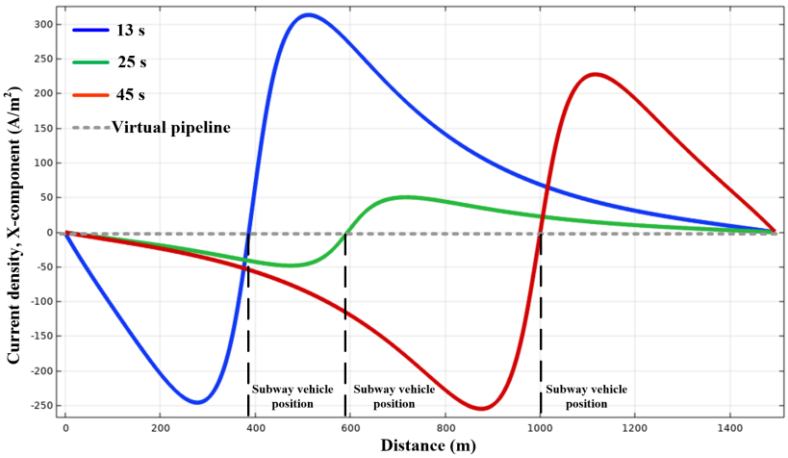

Figure 5. Stray current density flowing through the buried pipe (X-component (A/m^2))

Figure 5 shows the stray current density (X-component) flowing through the buried pipeline, with positive and negative current density values. The positive and negative current values indicate

that the current in the pipeline flows from the subway vehicle position in two opposite directions (the direction of the two stations). With current flowing in and out, the cathode and anode will be generated on the buried pipeline. The metal in the anodic area of the buried pipeline will be corroded with the loss of electrons [7,16]. During the movement of the subway vehicle, the current density flowing through the buried pipeline is constantly changing. During the acceleration phase (13 s) of subway vehicles, the maximum current density of the pipeline is as high as 312 A/m^2 (X-component). The mass loss of the metal due to corrosion will increase with increasing current flowing through the buried pipeline. Therefore, the possible metal corrosion caused by a small amount of stray current should not be ignored. The entire corrosion process of the metal anode under stray current will be discussed in detail in the following experiment.

3. EXPERIMENT

Due to the large scales of the subway interval and the dynamic characteristics of the subway vehicle, it is difficult to establish a complete experimental platform to verify the stray current distributions and corrosion behaviours of buried pipelines. To achieve a short cycle and reliable experimental requirements, an experimental platform for simulating soil corrosion on carbon steel specimens with a mixed solution was established. This experiment mainly observes the influence (anodic reaction and mass loss) of stray current on the corrosion of carbon steel specimens under a constant soil conductivity. An equal-scale experimental multi-physics coupled FEM model will be established to verify the experimental results in Section 4.

3.1 Experimental Preparation

N20 carbon steel is a commonly used as structural steel in buried urban gas pipelines and gas field stations [36]. N20 carbon steel belongs to the low carbon steel group and has a chemical composition of (wt.%): 0.21 C, 0.22 Si, 0.45 Mn, 0.04 P, 0.04 S, 0.014 Mg and 0.02 Cr. In this work, N20 carbon steel specimens were selected as the buried pipeline metal for stray current corrosion in the experiment, as shown in Figure 6. The experimental specimen was 120 mm in length, 25 mm in width, and 2 mm in thickness. Two circular holes with a diameter of 4 mm were placed in the centre of both ends in the longitudinal direction of the specimen (the centre distance was 5 mm from the width side) to facilitate fixing the specimen to different positions of the container with insulated ropes. Prior to the experiment, the surfaces of the experimental specimens were washed with absolute ethanol and water to wash away any remaining stain. Then, the cleaned specimens were dried and stored for use in the experiment. During the experiment, the soil environment was simulated with a mixed solution of Na_2SO_4, NaCl and $NaHCO_3$. The simulated soil solution was made up of 25 L water, 300 g NaCl, 150 g Na_2SO_4 and 50 g $NaHCO_3$, whose conductivity, measured by a conductivity metre (DDS-11A), was 1.5 S/m. The main ionic concentration of the simulated soil solution is shown in Table 1.

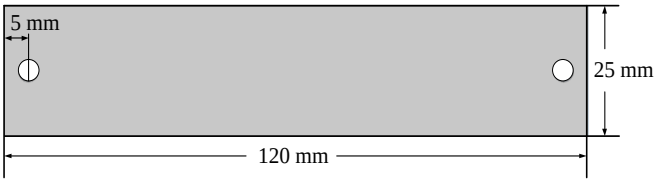

Figure 6. Size of the N20 carbon steel specimen

Table 1. Ion concentration of the simulated soil solution (g/L)

Na^+	Cl^-	SO_4^{2-}	HCO_3^-
7.21	7.29	4.06	1.45

3.2 Experimental design

Experiments were carried out on specimens of stray current, as shown in Figure 7. The 40×24×28 cm3 container was used to hold the simulated soil solution. The prepared N20 carbon steel specimens were fixed in the solution. The positive and negative poles of the programmable DC power supply (Henghui HCP-1022) were connected to a graphite rod electrode and a titanium rod electrode, respectively. The electrodes had a diameter of 8 mm and a length of 100 mm. The graphite rod electrode was regarded as the leakage point of the current, while the titanium rod electrode was regarded as the return point of the current. A current field was formed in the simulated soil solution when the power supply was turned on. In the current field, most of the current returned directly to the negative pole of the power supply through the solution. The other current returned to the negative pole of the power supply after passing through the carbon steel specimen fixed in the solution. Therefore, the experimental platform formed a corrosive environment similar to the conditions of a buried pipeline in a subway interval.

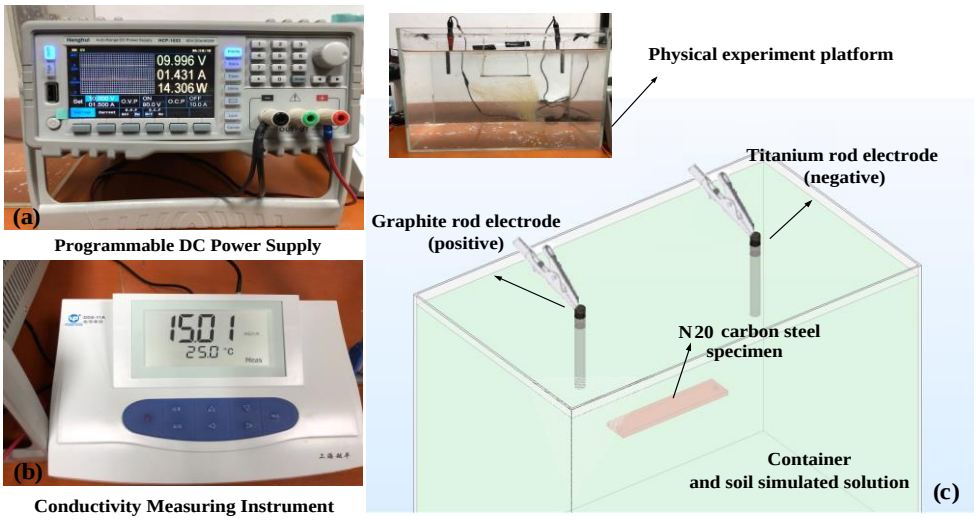

Figure 7. Instrument usage and physical experimental design

A total of three sets of buried metal corrosion experiments were set up at different depths. The first set of experimental carbon steel specimens was placed 50 mm from the upper surface of the solution, and the second and third experimental specimens were set to 100 mm and 150 mm, respectively. The programmable DC power supply voltage was set to 10 V, and the output current was approximately 1.4 A. The experiment lasted for 48 h in each group. After the experiment, the specimen was removed for rust removal and dried, and data on the mass loss of the specimen were recorded. It should be noted that during the experiment, the conductivity of the solution underwent minor changes. Considering that the experimental period was relatively short, the influence of the change in conductivity on the observed corrosion was ignored here.

4. EXPERIMENTAL THEORETICAL MODELLING

A multi-physics coupled FEM model was built in a 1:1 proportion to the experimental platform. The physics fields involved in the model were governed by equations from the constant electric field theory, the electrochemical theory and the transport theory of diluted species. The coupling process of the related theories for the modelling was as follows:

1) According to the constant electric field theory (charge transfer in the electrolyte obeys Ohm's law), the current supplied by the DC power source generated a current field in the solution (simulating the distribution of stray current in the soil).

2) With the current flowing in and out, the carbon steel specimen generated electrode reactions in the simulated soil solution (electrolyte). The anodic metal lost electrons during the electrode reaction, and the metal ions were dissolved in the simulated soil solution.

3) According to the mechanism of dilute substance transfer (electric field migration), the concentration of metal ions continuously accumulated during the electrode reaction, and the mass loss of metal under cumulative corrosion could be calculated.

4.1 Constant electric field distribution theory

The boundary conditions are consistent with the experimental platform. The positive graphite rod electrode of the FEM theoretical model applies a DC voltage of U_0=10 V, and the potential of the negative titanium rod electrode was set to 0 V. The solution is considered to be a homogeneous medium with uniform conductivity. The stray current field generated in the solution can also be controlled by Equations (1-3). The letters J_l and σ_l are used to represent the current density and conductivity of the simulated soil solution, respectively.

The area of the curved surface that is arbitrarily closed between the positive and negative poles is defined as *S*. According to Kirchhoff's current law, the current flowing into and out of *S* is equal, which is I_0.

$$I_0 = \int_S J_l \cdot dS \tag{4}$$

Other boundaries are defaulted to insulation boundary conditions：

$$n \cdot J_l = 0 \quad (5)$$

where n is the normal vector and points outside the domain of the model.

4.2 Electrochemical corrosion theory

In the theoretical model, the current in the specimen is calculated by the "Secondary Current Distribution" interface provided by the COMSOL Multiphysics software. The current density distributed on the specimen is J_{Fe}, which is derived from the current density J_l of the solution, and the relationship between the two is shown in Equation (6):

$$J_{Fe} = n \cdot J_l \quad (6)$$

The relationship between the local current density $J_{loc,Fe}$ and J_{Fe} of the specimen can be written as Equation (7):

$$\sum J_{loc,Fe} = J_{Fe} \quad (7)$$

According to the electrochemical theory, carbon steel specimens form electrodes in a simulated soil solutions that are energised. As seen in Figure 8, the region where the current flows into the specimen is the cathodic region, and the region where the current flows out of the specimen is the anodic region. In the modelling, the boundary of the specimen in the red dotted frame and the blue dotted frame are defined as the "anode" and "cathode", respectively.

The cathodic reaction is represented by a hydrogen evolution reaction without considering the acidity or alkalinity of the solution, and the reaction expression is:

$2H^+ + 2e^- \rightarrow H_2$

In the anodic region, the dissolution reaction of iron losing electrons and forming divalent iron ions is:

$Fe \rightarrow Fe^{2+} + 2e^-$

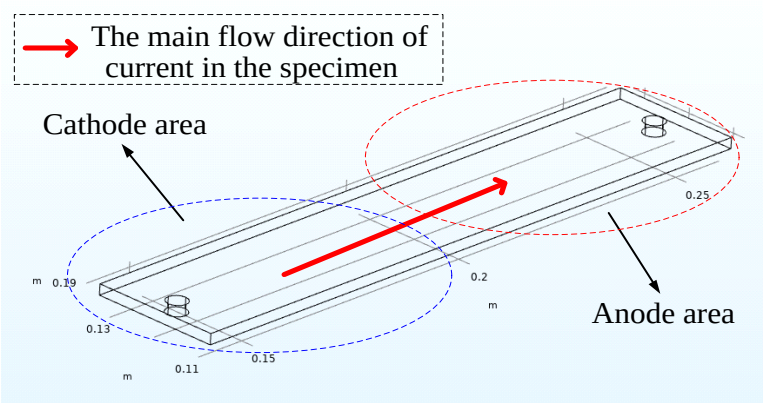

Figure 8. Distribution of specimen electrodes

Due to the distribution of current in the specimen and the self-resistance of the specimen, the potential in the carbon steel specimen can be obtained. Assuming that the electrode potential at the anode of the specimen is ϕ_{Fe}, the overpotential η_{Fe} at the interface between the electrode and the electrolyte can be written as Equation (8).

$$\eta_{Fe} = \phi_{Fe} - \phi_l - E_{eq,Fe} \quad (8)$$

where $E_{eq,Fe}$ is the equilibrium potential electrode reaction. Using the Butler-Volmer equation to simulate an anodic chemical reaction, the local current density can be calculated according to the following expression:

$$J_{loc,Fe} = J_{0,Fe}\left(\exp(\frac{\alpha_a F\eta_{Fe}}{RT}) - \exp(-\frac{\alpha_c F\eta_{Fe}}{RT})\right) \quad (9)$$

where $J_{0,Fe}$ is the exchange current density of the iron reaction, α_a and α_c represent the anodic charge transfer coefficient and the cathodic charge transfer coefficient, respectively, R represents the general gas constant, and F is the Faraday constant. The carbon steel corrosion rate can be obtained by Faraday's law:

$$v_{Fe} = \frac{M_{Fe} J_{loc,Fe}}{nF} \quad (10)$$

where M_{Fe} is the average molar mass of iron and n is the number of electrons lost by the iron reaction.

The hydrogen evolution reaction of the cathode can be simulated by the Tafel equation. Considering that the article focuses on the analysis of the anodic corrosion of metal, the cathodic reaction is not described in detail here.

4.3 Transport theory of diluted species

As the electrochemical reaction of the anode progresses, the ferrous ions generated by the reaction continuously diffuse and migrate in the soil simulation solution, and the ferrous ion concentration also changes. The process of ferrous ion transmission and accumulation can be simulated and analysed by the "Transport of Diluted Species" component provided by COMSOL Multiphysics software. The transport of iron ions can be described by the Nernst-Planck equation:

$$N_{Fe} = -D_{Fe}\nabla c_{Fe} - nu_{Fe}Fc_{Fe}\nabla\phi_l \quad (12)$$

where N_{Fe} is the transfer vector (mol/(m^2·s), c_{Fe} is the electrolyte concentration (mol/m^3), n is the number of charges carried by the ion, and u_{Fe} is the mobility of the charged species (m^2/s·J·mol).

The parameters involved during the FEM model calculation process are shown in Table 2.

Table 2. Electrochemical model parameters

Parameter name	Value	International unit	Description
F	96485	C/mol	Faraday constant
$E_{eq,Fe}$	- 0.76	V	Equilibrium potential
$J_{0,Fe}$	7.1×10^{-5}	A/m^2	Exchange current density

A_{Fe}	0.41	mV/decade	Ion Reduction Tafel Slope
M_{Fe}	56	g/mol	Average molar mass of iron
n	2	--	Electrons lost
σ_l	1.5	S/m	Electrolyte conductivity of the solution
α_a	1.5	--	Anode charge transfer coefficient
α_c	0.5	--	Cathode charge transfer coefficient
R	8.31	J/(mol·K）	General gas constant
D_{Fe}	2E-9	m^2/s	Diffusion coefficient
$c_{i0,Fe}$	1E-7	mol/m^3	Initial iron ion concentration
v_c	-1	--	Chemical equivalent coefficient

5. RESULTS AND DISCUSSION

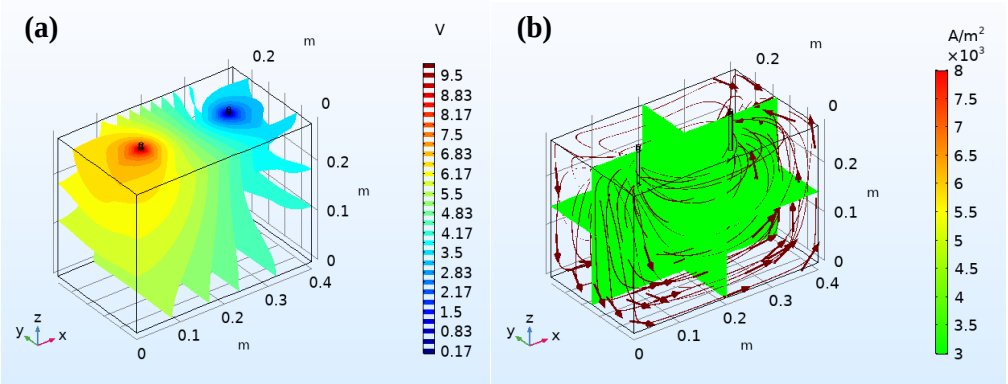

Figure 9. Constant electric field : (a) potential field and (b) current density

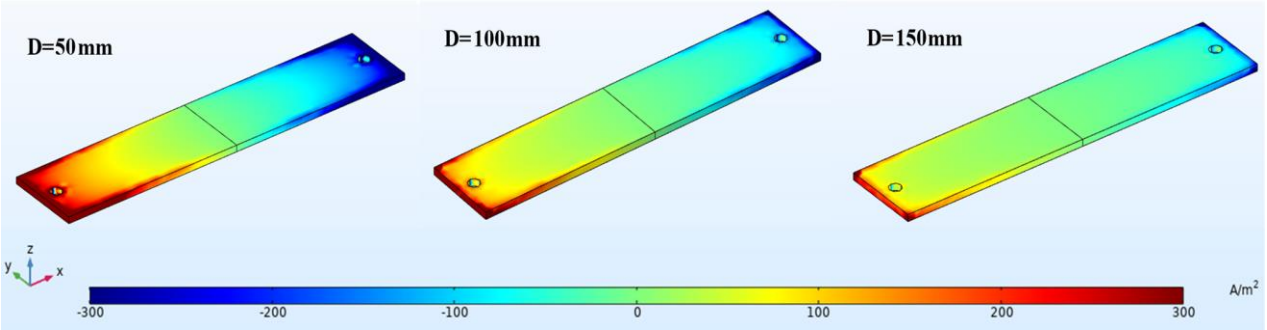

Figure 10. Local current densities of the specimens

In the conductive loop of this study, the potential field formed in the solution is shown in Figure 9(a), and the current density in the solution is shown in Figure 9(b). The maximum potential in the solution is 10 V, which is equal to the power supply voltage. The potential distribution gradually decreases from the positive electrode to the negative electrode, and the equipotential surfaces are

symmetrically distributed on the left and right sides of the 5 V potential surface. The current flowing from the positive electrode of the power supply is returned to the negative electrode through the soil solution. The current density is the highest at the positive and negative terminals of the power supply, and the current density at other locations decreases as it goes away from the power supply.

As shown in Figure 10, in the three sets of multi-physics coupled FEM models, the burial depths of the specimens were 50 mm, 100 mm and 150 mm. Comparing the colours of the three specimens, it is obvious that the local current densities of the three specimens are different. The deeper the burial depth, the lighter the colour, indicating that the local current density of the specimen is smaller. The positive current density (red area) indicates that the current flows into the specimen, while the negative value (blue area) indicates that the current flows out of the specimen. The positive current density area and negative current density area of the specimen are almost symmetrically distributed, which demonstrates Kirchhoff's current law: the current flowing into the closed area is equal to the current flowing out.

The multi-physics coupled FEM model calculates the corrosion rate of each point on the surface (anodic area) of the specimen in reference to Equation (11). The overall corrosion rate of the specimen is obtained by integrating the corrosion rate at each point, which can be seen in Figure 11(a). When the buried depth of the specimen is 50 mm, the corrosion rate is the largest, with a value of approximately 0.1008 g/h. In the simulation process, the change in the conductivity of the solution and the accumulation of corrosive substances are neglected, so the corrosion rate remains basically unchanged. When the specimen depth is 100 mm and 150 mm, the corrosion rates are 0.0541 g/h and 0.0332 g/h, respectively. During the simulation, the time unit is selected to be an hour, and the time steps are 0, 0.5, and 48 h.

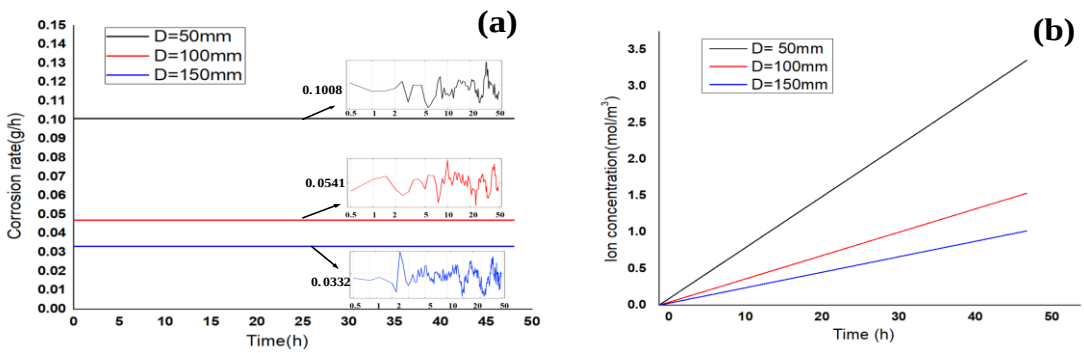

Figure 11. (a) Corrosion rate of the specimens and (b) ion concentration of the specimens

The local corrosion or pitting process of metal must be accompanied by ion transfer [37]. The ferrous ions gradually increase in the solution in relation to the corrosion of the specimen. The concentration c_{Fe} of ferrous ions can be controlled by Equation (12). Figure 11(b) is a graph showing the accumulation of ferrous ions in specimens with different burial depths in solution. After 48 h, the ferrous ion concentrations in the three simulated soils (50 mm, 100 mm and 150 mm) were 3.355 mol/m^3, 1.533 mol/m^3 and 1.018 mol/m^3, respectively. The simulation results of the ferrous ion concentrations on the surfaces of the specimens are shown in Figure 13. From Figure 13, we can see that the ferrous ions are mainly concentrated in the anodic area of the specimens. When close to the

anodes, the ferrous ion concentration is increased. In general, the ferrous ion concentration is inversely proportional to the depth of the specimen.

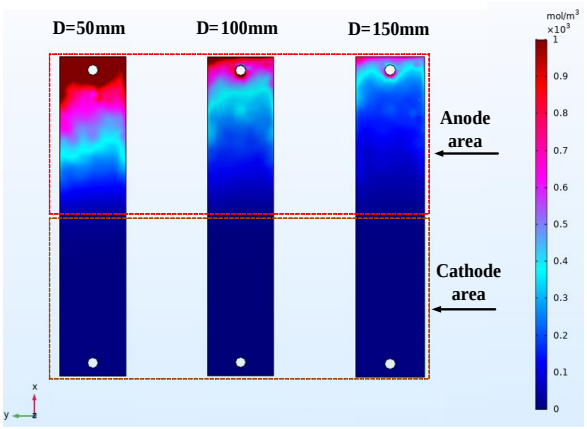

Figure 12. Ferrous ion concentration (top view)

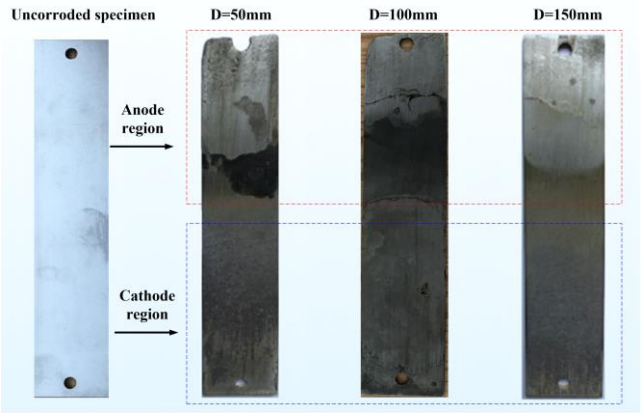

Figure 13. Experimental corrosion results

Figure 13 shows the corrosion results of the three sets of specimens involved in the experiments. The corrosion trends demonstrated in the experimental results and in the simulation specimens are the same. The most corrosion occurs in the anodic area of the specimens; moreover, when the stray current gets closer to the anode, the corrosion becomes more severe. There is almost no corrosion of the cathode specimens. The experimental and simulation data of specimen mass losses are shown in Table 3. It can be seen that there is a certain error between the simulation data and the experimental data. The results show that the relative error between the experimental value and the simulation value increases as the depth of the specimen increases. During the experiment, the solution concentration, conductivity, and other parameters are constantly changing. These changes are completely ignored in the simulation, so deviations between the experiment and simulation results are inevitable. In general, the relationship between the corrosion rate and current density follows a linear rule in the corrosion experiment, which is consistent with the results of metal corrosion weight loss

analysis by other scholars [25, 38]. The FEM calculation is convenient to simulate the process of electrochemical corrosion, and provides an efficient method for stray current corrosion research [39, 40]. The similar FEM simulation and experimental methods have been previously used to study the stray current corrosion of reinforced concrete in rail transit system [41, 42].

Table 3. Experimental and simulation data

Specimen depth (mm)	50	100	150
Experimental mass loss (g)	4.75	2.24	1.52
Simulation mass loss (g)	4.70	2.15	1.43
Relative error value	1.05%	4.02%	5.92%

6. CONCLUSIONS

Based on the actual operation of subway vehicles in a subway interval, a three-dimensional finite model was established to analyse the stray current distribution in the subway area and the corrosion interference to buried pipelines. A corrosion experiment of N20 carbon steel that simulates stray current corrosion was carried out. The course of the corrosion experiment was simulated by establishing another FEM model. Three critical conclusions have been highlighted as follows:

1) The simulation results for the 3D-finite element model with the particular subway interval show that the influence of the stray current of the subway on the buried pipeline is directly related to the location of the buried pipeline. The buried pipeline near the subway vehicle, where the pipeline has the greatest potential to ground, is more vulnerable to corrosion. The maximum potential value (0.075 V) of the buried pipeline to ground is far less than the protection standard (0.3 V), but the long-term corrosion effect of stray current cannot be ignored.

2) The simulation results are basically consistent with the experimental results (corroded areas and mass loss) of N20 carbon steel specimens. The simulation results can accurately reflect the electrochemical corrosion law: the current flows out from the anodic surfaces of the specimens, and the stray current corrosion of the metal is mainly concentrated in the anodic area, which has local characteristics. The experimental value and the simulated value of the mass loss due to corrosion of the specimens are basically the same (the minimum relative error is only 1.05%), which indicates that the finite element model is feasible for quantitative calculation of metal corrosion.

3) The theoretical modelling and quantitative calculation of simulated stray current corrosion provide a direct calculation tool for stray current corrosion on the metal of buried pipelines. The corrosion model of carbon steel specimens can be extended to the subway interval model, and the corrosion degree and the service life of buried metal near the subway line can be predicted.

FUNDING
This research was funded by National Natural Science Foundation of China under Grant 51807065.

CONFLICTS OF INTEREST
The authors declare no conflict of interest.

References

1. K. K. Tang, *Corros. Sci.*, 152 (2019) 153.
2. Y. Tzeng and C. Lee, *IEEE Trans. Power Deliv.*, 25 (2010) 1516.
3. Z. Chen, D. Koleva, K.van. Breugel, *Corros. Rev.*, 36 (2017) 1.
4. C. T. Wang, W. Li, Y. Q. Wang, S. Y. Xu, M. B. Fan, *Int. J. Electrochem. Sci.*, 13 (2018) 1700.
5. C. A. Charalambous and P. Aylott, *IEEE Trans. Veh. Technol.*, 63 (2014) 3530.
6. C. A. Charalambous, I. Cotton and P. Aylott, *IEEE Trans. Power Del.*, 28 (2013) 1899.
7. L. Bertolini, M. Carsana and P. Pedeferri, *Corros. Sci.*, 49 (2007) 1056.
8. A. Zaboli, B. Vahidi, S. Yousefi and M. M. Hosseini-Biyouki, *IEEE Trans. Veh. Technol.*, 66 (2017) 974.
9. National Physical Laboratory (UK), Estimate of annual costs attributable to corrosion of reinforced concrete structures in the United Kingdom. www.npl.co.uk. (Accessed 18 November 2016).
10. Y. C. Li, C. Xu, R. H. Zhang, Q. Liu, X. H. Wang and Y. C. Chen, *Int. J. Electrochem. Sci.*, 12 (2017) 1829.
11. W. Li, Stray current Corrosion Monitoring and Protection Technology in DC Mass Transit Systems, *China Univ. Mining/Tchnol. Press.*, (2004) Xuzhou, China.
12. A. Cerman, F. Janicek, M. Kubala, Resistive-type network model of stray current distribution in railway DC traction system, 16th International Scientific Conference on Electric Power Engineering IEEE, 2015, 364-368.
13. A. Ogunsola, L. Sandrolini, A. Mariscotti, *IEEE Trans. Ind. Appl.*, 51 (2015) 5431.
14. C. A. Charalambous, *IEEE Trans. Veh. Technol.*, 66 (2017) 9667.
15. H. W. M. Smulders and M. F. P. Janssen, Modeling d. c. Stray Currents Using a Multi-Layer Model, Proceedings of the 7th World Congress on Railway Research, Montréal, Canada, 2006.
16. G. X. Li, D. L. Zhang, Y. Wu and H. Liao, *Int. J. Adv. Comput. Technol.*, 5 (2013) 37.
17. G. Cao, Q. Gu, Y. Jiang, Y Li, et al, *Nat. Gas Ind. B.*, 6 (2019) 427.
18. I. Cotton, C. Charalambous, P. Aylott and P. Ernst, *IEEE Trans. Veh. Technol.*, 54 (2005) 722.
19. Z. C. Cai, X. W. Zhang, H. Cheng, *IEEE Access*, 7 (2019) 168404.
20. Chuchit, T. & Kulworawanichpong, T. *Electr Eng.*, 101 (2019) 81.
21. A. Zaboli, B. Vahidi, S. Yousefi, M. M. Hosseini-Biyouki, *IEEE Trans. Veh. Technol.*, 66 (2017) 974.
22. Q. Y. Qin, B. X. Wei, Y. L. Bai, L. Nan, J. Xu, C. K. Yu, C. Sun, *Int. J. Pressure Vessels Piping.*, 179 (2020) 104016.
23. C. T. Wang, W. Li, Y. Q. Wang, S. Y. Xu, X. F. Yang, *Const. Build. Mater.*, 219 (2019) 164.
24. E. Mahdi, A. Rauf, E.O. Eltai, *Corros. Sci.*,83 (2014) 48.
25. X. H. Wang, X. T. Song, Y. C. Chen, Z. Q. Wang, *Int. J. Electrochem. Sci.*, 13 (2018) 5654.
26. F. Xie, D. Wang, C. X. Yu, Y. Zong, M. Wu, *Int. J. Electrochem. Sci.*, 12 (2017) 9565.
27. F. L. Ma, R. Z. Xie, P. J. Hua, X. H. Bai, *Int. J. Electrochem. Sci.*, 13 (2018) 5396.
28. H. M. Qin, Y. X. Du, M. X. Lu, Q. S, Meng, *Mater. Corros.*, (2019) 1.
29. P. J. Han, R. Z. Xie, R. Liu, B. He, X. H. Bai, P. Han, *Const. Build. Mater.*, 12 (2019), 7668.
30. A. O. S. Solgarrd, M. Carsana, M. R. Geiker, A. Küter, L.Bertolini, *Corros. Sci.*, 74 (2013) 1.
31. Y. F. Wang, G. X. Cheng, Y. Li, *Corros. Sci.*, 111 (2016) 508.
32. D. Y. Wang, M. Z. W. Zhu, N. F. Wang, D. Zhu, H. G. Rui, *Electrochim. Acta*, 156 (2015) 301.
33. J. Du, J. H. Guo, L. Q. Zhao, Y. X. Chen, C. L. Liu, X. H. Meng, *Int. J. Electrochem. Sci.*, 13 (2018) 5810.

34. J. Newman, *J*. Electrochem. *Soc.*, 138 (1991) 3557.
35. 36.BS EN50162-2004, Standards Policy and Strategy Committee. Protection against Corrosion by Stray Current from Direct Current Systems [S]. London: BSI, 2005.
36. A. H. Liu, J. Y. Chen, F. T. Liang, S. Z. Chen, W. B. Chen, *Corros. Sci. Prot. Technol.*, 31 (2019) 52.
37. R. Montoya, J. C. Galvan, J. Genesca, *Corros. Sci.*, 53 (2011) 1806.
38. C. Wen, J. B. Li, S. L. Wang, Y. Yang, *J. Nat. Gas Sci. Eng.*, 27 (2015) 1555.
39. W. J. Mai, S. S. Soghrati, G. Buchheit, *Corros. Sci.*, 110 (2016) 157.
40. L. T. Yin, Y. Jin, C. Leygraaf, J. Pan, *Electrochimica. Acta*, 192 (2016) 310.
41. Y. Hong, Z. H. Li, G. F. Qiao, J. P. Ou, *Const. Build. Mater.*, 157 (2017) 416.
42. K. K. Tang, *Mater. Today. Commun.*, 20 (2019) 100564.